Finite-Element Analysis of Unsteady Incompressible Flow around an Oscillating Obstacle of Arbitrary Shape

THEODORE BRATANOW,* AKIN ECER,† AND MICHAEL KOBISKE‡
University of Wisconsin, Milwaukee, Wis.

An analytical method based on the Navier-Stokes equation was developed for representing unsteady flow around oscillating obstacles. A variational formulation of the Helmholtz vorticity equation was discretized in finite element form and integrated numerically. At each step of the numerical integration the velocity field around the obstacle was determined from the finite solution of Poisson's equation. The time-dependent boundary conditions around the oscillating obstacle were introduced as external constraints at each step of the numerical integration. The obtained results for a cylinder and an airfoil were illustrated in the form of streamlines and vorticity and pressure distributions.

Nomenclature

A = area of a triangular element, in.^{2} (m^2)
$\mathbf{b}$ = vector representing the boundary conditions around the obstacle
$\mathbf{c}$ = vector representing the boundary conditions at the freestream boundary
$\mathbf{F}$ = vector representing body forces, lbf (N)
$\mathbf{h}$ = vector representing the right-hand side of Eqs. (20–22)
$\mathbf{p}$ = vector representing nodal pressures for the finite element gridwork, lbf/in.^{2} (N/m^2)
p = pressure, lbf/in.^{2} (N/m^2)
$\mathbf{S}$ = a square matrix derived for the left-hand side of Eqs. (20–22)
$\mathbf{U}, \mathbf{V}$ = vectors representing the nodal velocities for each element in x and y directions respectively, in./sec (m/sec)
u, v = velocities in x and y directions, in./sec (m/sec)
$\mathbf{u}$ = velocity vector, $\mathbf{u} = [uv]$, in./sec (m/sec)
$\mathbf{W}$ = vector representing the nodal vorticities for each element, sec^{-1}
$\boldsymbol{\delta}$ = vector representing Lagrange multipliers
δ_i = a Lagrange multiplier
ν = kinematic viscosity of the fluid, in.^{2}/sec (m^2/sec)
ρ = density of the fluid, lbm/in.^{3} (Kg/m^3)
Φ_i = a quadratic functional
ψ = streamfunction, in.^{2}/sec (m^2/sec)
$\boldsymbol{\psi}$ = representing nodal streamfunctions and velocities
ω = vorticity, sec^{-1}
$\boldsymbol{\omega}$ = vorticity vector in x, y, z directions, sec^{-1}

Subscripts
b = at the obstacle boundary
c = at the freestream boundary
g = for a triangular element
p = for pressures
s = for streamfunctions and velocities
x, y = for derivatives with respect to x and y
ω = for vorticities
0 = at time t_0

Introduction

THE Navier-Stokes equations can describe a large class of time-dependent flow problems. Due to the involved nonlinearities, solutions of these equations have often been restricted to idealized cases. Numerical solutions of the Navier-Stokes equations, utilizing high-speed computers, have been developed by numerous investigators.[1-4] Such solutions have been based to a large extent on finite-difference techniques. The obtained results have demonstrated the advantages of the finite-difference method; however, the applications have been limited due to complexities in the developed computational procedures.

In an effort to overcome some of these difficulties, the finite element method, developed initially for solid mechanics,[5] has been applied to a number of fluid flow problems.[6,7] The present analysis is an application of the finite element method to two-dimensional, unsteady, incompressible viscous flow about oscillating obstacles of arbitrary shape. The developed mathematical model was based on a discrete variational formulation of the vorticity transport equation in terms of vorticities and streamfunctions. The analysis extends previous application of finite element procedures in two main areas. One is concerned with the boundary conditions around the oscillating obstacle; the other with a local linearization of the nonlinear terms in the governing differential equations so that the variational functionals can be defined. A much more detailed description of this analysis and of prior use of finite element methods in fluid mechanics is presented in Refs. 8 and 9.

Mathematical Background

The two-dimensional Navier-Stokes equations for analyzing the motion of incompressible fluids can be written as

$$(\partial\mathbf{u}/\partial t)+(\mathbf{u}\cdot\mathbf{V})\mathbf{u} = (1/\rho)\mathbf{F}-(1/\rho)\mathbf{V}p+\nu\nabla^2\mathbf{u} \tag{1}$$

The equation of continuity for incompressible fluids is

$$\mathbf{V}\cdot\mathbf{u} = 0 \tag{2}$$

The vorticity and streamfunctions can be defined respectively as

$$\omega = \mathbf{V}\times\mathbf{u} \tag{3}$$

and

$$\mathbf{u} = [\psi_y \quad -\psi_x] \tag{4}$$

The vorticity transport equation is then derived from Eqs. (1–3) as

$$(\partial\omega/\partial t)+(\mathbf{u}\cdot\mathbf{V})\omega = \nu\nabla^2\omega \tag{5}$$

From Eqs. (3) and (4) the streamfunctions are related to vorticity as follows:

$$\nabla^2\psi = -\omega \tag{6}$$

The pressure distribution for a given velocity field can be calculated from the supplementary equation

$$\nabla^2 p = -\rho Q \tag{7}$$

where

Presented as Paper 73-91 at the AIAA 11th Aerospace Sciences Meeting, Washington, D.C., January 10–12, 1973; submitted February 20, 1973; revision received July 10, 1973. This research was supported by NASA under grant NGR-50-007-001.

Index category: Nonsteady Aerodynamics.

* Professor of Engineering Mechanics. Member AIAA.
† Assistant Professor of Engineering Mechanics. Member AIAA.
‡ Research Assistant.

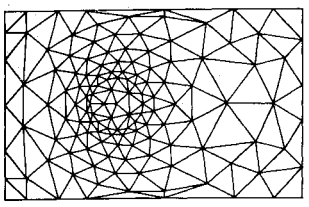

Fig. 1 Finite element gridwork for cylinder.

$$Q = 2(u_y v_x - u_x v_y) \tag{8}$$

The analysis of incompressible, unsteady, viscous flow involves the simultaneous solution of Eqs. (5) and (6) and numerical integration of Eq. (6). The pressure distribution at any time interval can be calculated from Eq. (7).

Finite-Element Analysis

The finite-element method was applied for the numerical solution of Eqs. (5–7) under time-dependent boundary conditions. The developed procedure is efficient in dealing with the nonlinear terms in these equations and in representing the time-dependent boundary conditions around an oscillating obstacle of arbitrary shape. The steps of the analytical procedure are summarized below.

Variational Formulation

If the differential equations were all linear the variational formulation would be straightforward. The exact variational formulation of the vorticity transport equation can not be obtained because of the nonlinear convective terms. However, these terms can be linearized using a Taylor series expansion of velocities in terms of vorticities. The velocity at time $t_0+\Delta t$ can be written as

$$\mathbf{u} = \mathbf{u}_0 + (\partial \mathbf{u}/\partial \omega)_0 \, d\omega + 1/2!(\partial^2 \mathbf{u}/\partial \omega^2)_0 (d\omega)^2 + \ldots \tag{9}$$

The instantaneous gradient of the velocity field can be calculated from the discretized finite element model. The variational functional for the vorticity transport equation can be written as follows

$$\Phi_3 = \int_A \omega \frac{\partial \omega}{\partial t} dA + \frac{1}{2}\int_A [u\omega\omega_x + v\omega\omega_y] dA + \frac{v}{2}\int_A [\omega_x^2 + \omega_y^2] dA \tag{10}$$

Eqs. (6) and (7) are in the form of Poisson's equation, for which a direct variational formulation exists. The solutions of Eqs. (6) and (7) can be obtained by minimizing the functionals

$$\Phi_1 = \frac{1}{2}\int_A \{\psi_x^2 + \psi_y^2\} dA - \int_A \omega\psi \, dA \tag{11}$$

and

$$\Phi_2 = \frac{1}{2}\int_A \{p_x^2 + p_y^2\} dA - \int_A \rho p Q \, dA \tag{12}$$

under corresponding boundary conditions. The solutions of Eqs. (5–7) can be obtained by minimizing Eqs. (10–12), respectively. A discrete finite element model was used for this purpose.

Finite-Element Model

The obstacle and the surrounding continuum were represented by discrete finite elements as shown in Figs. 1 and 2. For a stationary obstacle, a finer gridwork was arranged for the regions where the variation of velocity is more pronounced. For a moving obstacle, the gridwork was arranged more uniformly, as seen in Fig. 2. In both cases the finite-element grid represents a stationary space in the continuum in which the obstacle moves. The position of the moving obstacle in this space is defined at discrete time intervals. Accordingly, the major portion of the governing discretized equations, corresponding to the flowfield without the obstacle, does not change. This reduces the computational effort considerably.

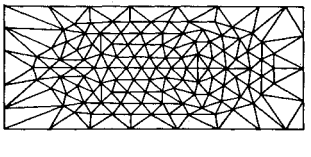

Fig. 2 Finite element gridwork for airfoil.

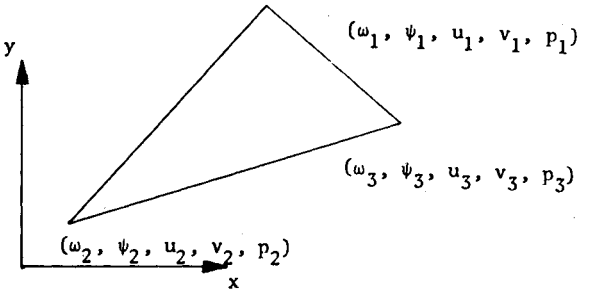

Fig. 3 A typical triangular finite element.

Different finite-element models were chosen for representing the variations of streamfunctions, vorticies and pressures. For a typical finite element, shown in Fig. 3, the vorticities and pressures were assumed to vary linearly over each finite element as

$$\omega(x,y) = [\xi_1 \xi_2 \xi_3] \begin{bmatrix} \omega_1 \\ \omega_2 \\ \omega_3 \end{bmatrix} = \mathbf{BW}^g \tag{13}$$

$$p(x,y) = [\xi_1 \xi_2 \xi_3] \begin{bmatrix} p_1 \\ p_2 \\ p_3 \end{bmatrix} = \mathbf{Bp}^g \tag{14}$$

where ξ_1 are the area coordinates of a finite element. For the steamfunctions a third-order variation was assumed as follows

$$\psi = \mathbf{CA}\psi^g \tag{15}$$

where

$$\mathbf{C} = [\xi_1^3 \xi_2^3 \xi_3^3 \xi_1^2\xi_2 \xi_1^2\xi_3 \xi_2^2\xi_3 \xi_2^2\xi_1 \xi_3^2\xi_1 \xi_3^2\xi_2 \xi_1\xi_2\xi_3] \tag{16}$$

and

$$\psi^{gt} = [\psi_1 \psi_{1x} \psi_{1y} \psi_2 \psi_{2x} \psi_{2y} \psi_3 \psi_{3x} \psi_{3y}] \tag{17}$$

where vector ψ represents the streamfunctions and velocities at the nodes of a triangle. Matrix $\mathbf{A}$ is defined as

$$\mathbf{A} = \begin{bmatrix} 1 & 0 & 0 & 0 & 0 & 0 & 0 & 0 & 0 \\ 0 & 0 & 0 & 1 & 0 & 0 & 0 & 0 & 0 \\ 0 & 0 & 0 & 0 & 0 & 0 & 1 & 0 & 0 \\ 3 & x_{21} & -y_{12} & 0 & 0 & 0 & 0 & 0 & 0 \\ 3 & -x_{13} & y_{31} & 0 & 0 & 0 & 0 & 0 & 0 \\ 0 & 0 & 0 & 3 & x_{32} & -y_{23} & 0 & 0 & 0 \\ 0 & 0 & 0 & 3 & -x_{21} & y_{12} & 0 & 0 & 0 \\ 0 & 0 & 0 & 0 & 0 & 0 & 3 & x_{13} & -y_{31} \\ 0 & 0 & 0 & 0 & 0 & 0 & 3 & -x_{32} & y_{23} \\ 2 & -\frac{3}{2}x_1 & -\frac{3}{2}y_1 & 2 & -\frac{3}{2}x_2 & -\frac{3}{2}y_2 & 2 & -\frac{3}{2}x_3 & -\frac{3}{2}y_3 \end{bmatrix} \tag{18}$$

where

$$x_{mn} = x_m - x_n \qquad y_{mn} = y_m - y_n \tag{19}$$

This matrix was developed for a plate bending element as described by Zienkiewicz et al.[10]

The finite-element models were employed in discretizing the variational functionals in Eqs. (9, 10, and 12). After minimizing

these functionals with respect to values of streamfunctions, vorticities and pressures at nodal points, the discretized form of Eqs. (5–7) were obtained as

$$\left[\sum_g \int_A \mathbf{B}^t\mathbf{B}\,dA\right]\frac{\partial \mathbf{W}}{\partial t} = \left[\sum_g - \int_A \{\nu[\mathbf{B}_x{}^t\mathbf{B}_x + \mathbf{B}_y{}^t\mathbf{B}_y] + \mathbf{B}^t\mathbf{B}\mathbf{U}\mathbf{B}_x + \mathbf{B}^t\mathbf{B}\mathbf{V}\mathbf{B}_y\}\,dA\right]\mathbf{W} \tag{20}$$

$$\left[\sum_g \int_A [\mathbf{A}^t\mathbf{C}_x{}^t\mathbf{C}_x\mathbf{A} + \mathbf{A}^t\mathbf{C}_y{}^t\mathbf{C}_y\mathbf{A}]\,dA\right]\boldsymbol{\psi} = \left[\sum_g \int_A [\mathbf{A}^t\mathbf{C}^t\mathbf{B}]\,dA\right]\mathbf{W} \tag{21}$$

$$\left[\sum_g \int_A [\mathbf{B}_x{}^t\mathbf{B}_x + \mathbf{B}_y{}^t\mathbf{B}_y]\,dA\right]\mathbf{P} = {}'\rho\sum_g \int_A [\mathbf{Q}\mathbf{B}]\,dA \tag{22}$$

The nonlinear convection terms in Eq. (20) were calculated using a Taylor series in terms of nodal vorticities as

$$\psi = \psi_0 + (\partial\omega/\partial W_i)_0\,dW_i + 1/2!(\partial^2\psi/\partial W_i\,\partial W_j)_0\,dW_i\,dW_j + \ldots \tag{23}$$

The instantaneous derivatives with respect to vorticities of both the streamfunctions and velocities can be calculated from Eq. (6).

Boundary Conditions

The boundary conditions for Eqs. (5–7) were introduced in the variational formulation of these equations as external constraints, using the Lagrange multiplier technique. For all three equations the boundary conditions

$$C_i(x, y) = 0 \tag{24}$$

were satisfied by minimizing the functional

$$\bar{\Phi} = \Phi + \delta_i C_i \tag{25}$$

The introduction of this technique increases the efficiency and flexibility of the numerical method since the boundary conditions can be defined in time and space in a most general manner. Considering the difficulties related to the boundary conditions encountered in the numerical analysis of flow problems using finite-difference techniques, this is a new and outstanding feature of the presented method.

The boundary conditions for streamfunctions, vorticities, and pressures were described at the boundary of the outer rectangle in Figs. 1 and 2, by defining the freestream conditions. These boundary conditions do not change during the numerical integration of the vorticity transport equation. The time-dependent boundary conditions on the surface of a stationary obstacle were defined at a series of points on the surface by specifying: 1) Streamfunctions have equal values and tangential velocities are equal to zero. 2) Vorticities are equal to the normal gradient of the tangential velocity component. 3) Pressure gradient normal to the obstacle surface is equal to zero. For an oscillating obstacle, the instantaneous velocities of fluid particles contacting the series of points on the obstacle surface were made equal to the velocities of these points. Streamfunctions were defined in a similar fashion.

Solution of the Equations

The numerical solutions of Eqs. (20–22) were developed in an identical computational format. During the numerical integration of Eq. (20) the time-dependent terms, representing the obstacle boundary conditions, were separated from the remaining terms in the equation. Such separate treatment increased the effectiveness of the computational procedure.

The boundary conditions corresponding to Eq. (6) can be considered as an additional constraint condition

$$\mathbf{c}_s{}^t\boldsymbol{\psi} = \mathbf{d}_s \tag{26}$$

at the freestream boundaries and

$$\mathbf{b}_s{}^t\boldsymbol{\psi} = \mathbf{e}_s \tag{27}$$

for the obstacle surface. The system of equations resulting from Eqs. (19, 23, and 24) can be written in matrix form as

$$\begin{bmatrix} \mathbf{S}_s & \mathbf{c}_s & \mathbf{b}_s \\ \mathbf{c}_s{}^t & \mathbf{0} & \mathbf{0} \\ \mathbf{b}_s{}^t & \mathbf{0} & \mathbf{0} \end{bmatrix}\begin{bmatrix} \boldsymbol{\psi} \\ \delta_{cs} \\ \delta_{bs} \end{bmatrix} = \begin{bmatrix} \mathbf{h}_s \\ \mathbf{d}_s \\ \mathbf{e}_s \end{bmatrix} \tag{28}$$

The matrices $\mathbf{S}_s$, $\mathbf{c}_s$, and $\mathbf{d}_s$ remain constant during the numerical integration, while matrix $\mathbf{b}_s$ changes depending on the instantaneous position of the obstacle. The combination of the constant matrices leads to

$$\begin{bmatrix} \mathbf{S}^* & \mathbf{b}_s{}^* \\ \mathbf{b}_s{}^{*t} & \mathbf{0} \end{bmatrix}\begin{bmatrix} \boldsymbol{\psi}^* \\ \delta_{bs} \end{bmatrix} = \begin{bmatrix} \mathbf{h}_s{}^* \\ \mathbf{e}_s \end{bmatrix} \tag{29}$$

where

$$\mathbf{S}^* = \begin{bmatrix} \mathbf{S} & \mathbf{c}_s \\ \mathbf{c}_s{}^{*t} & \mathbf{0} \end{bmatrix},\quad \mathbf{b}_s{}^* = \begin{bmatrix} \mathbf{b}_s \\ \mathbf{0} \end{bmatrix}$$
$$\mathbf{h}_s{}^* = \begin{bmatrix} \mathbf{h}_s \\ \mathbf{d}_s \end{bmatrix},\quad \boldsymbol{\psi}^* = \begin{bmatrix} \boldsymbol{\psi} \\ \delta_{cs} \end{bmatrix} \tag{30}$$

In Eq. (29) δ_{bs} is a column vector of Lagrange multipliers corresponding to the boundary conditions on the obstacle. The solution vector $\boldsymbol{\psi}^*$ can be written as

$$\boldsymbol{\psi}^* = \mathbf{q}_s - \mathbf{r}_s(\mathbf{b}_s{}^{*t}\mathbf{r}_s)^{-1}(\mathbf{b}_s{}^{*t}\mathbf{q}_s - \mathbf{e}_s) \tag{31}$$

where

$$\mathbf{q}_s = \mathbf{S}^{*-1}\mathbf{h}_s{}^* \tag{32}$$

$$\mathbf{r}_s = \mathbf{S}^{*-1}\mathbf{b}_s{}^* \tag{33}$$

Since matrix $\mathbf{S}^*$ is constant for a defined finite element gridwork, it is assembled and inverted only once. The obstacle is inserted into the flowfield by redefining vectors $\mathbf{b}_s$ and $\mathbf{e}_s$ at each time step. The steady and unsteady effects of the obstacle corresponding to its angle of attack and its motion are represented by vectors $\mathbf{b}_s{}^{*t}\mathbf{q}_s$ and $\mathbf{e}_s$, respectively. In the case of stationary object, matrices $\mathbf{b}_s$ and $\mathbf{r}_s$ are constant and vector $\mathbf{e}_s$ is equal to zero. For this case, only vectors $\mathbf{h}_s$ and $\mathbf{q}_s$ have to be redefined at each time step.

The boundary conditions for vorticities can be written in a similar manner as

$$\mathbf{c}_\omega{}^t(d\mathbf{W}/dt) = \mathbf{0} \qquad \mathbf{b}_\omega{}^t(d\mathbf{W}/dt) = \mathbf{e}_\omega \tag{34}$$

and the solution of Eq. (20) becomes

$$(d\mathbf{W}^*/dt) = \mathbf{q}_\omega - \mathbf{r}_\omega(\mathbf{b}_\omega{}^{*t}\mathbf{r}_\omega)^{-1}(\mathbf{b}_\omega{}^{*t}\mathbf{q}_\omega - \mathbf{e}_\omega) \tag{35}$$

The boundary conditions for the pressure solution from Eq. (22) are

$$\mathbf{c}_p{}^t\mathbf{P} = \mathbf{0} \qquad \mathbf{b}_p{}^t\mathbf{P} = \mathbf{0} \tag{36}$$

from which

$$\mathbf{P}^* = \mathbf{q}_p - \mathbf{r}_p(\mathbf{b}_p{}^{*t}\mathbf{r}_p)^{-1}(\mathbf{b}_p{}^{*t}\mathbf{q}_p) \tag{37}$$

Numerical Integration of the Vorticity Transport Equation

The time derivative of the vorticity vector given in Eq. (35) was numerically integrated to determine the unsteady behavior of the flow. At each time step of this numerical integration, the time derivative of the vorticity distribution was calculated from the solution of Eqs. (31) and (35). Different numerical integration techniques can be used for obtaining the desired accuracy. The selection of time step depends on the Reynolds number and the speed of the oscillatory motion of the obstacle.

At the beginning of the numerical integration of Eq. (35), the vorticity distribution was assumed to be zero for the entire flowfield. From this starting condition, vorticities were generated around the obstacle from Eq. (35) during the numerical integration corresponding to the boundary conditions described in Eq. (34). An under-relaxation factor was used on vector $\mathbf{e}_\omega$ in Eq. (35) for the first few steps of the integration. With the vorticity distribution determined at each time step, the streamfunctions and velocities were calculated from Eq. (31). Pressures were calculated at desired time steps from Eq. (37). The steady flow around a fixed obstacle was obtained by continuing the numerical integration until a steady state was reached. The steady-state vorticity distribution was then used as a starting condition for the analysis of flow around oscillating obstacles.

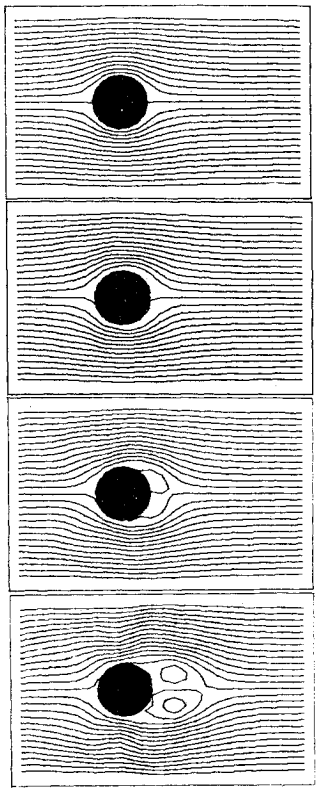

Fig. 4a Streamlines around a circular cylinder ($Re = 10^3$, $t = 0.2, 2.0, 3.4, 6.8$).

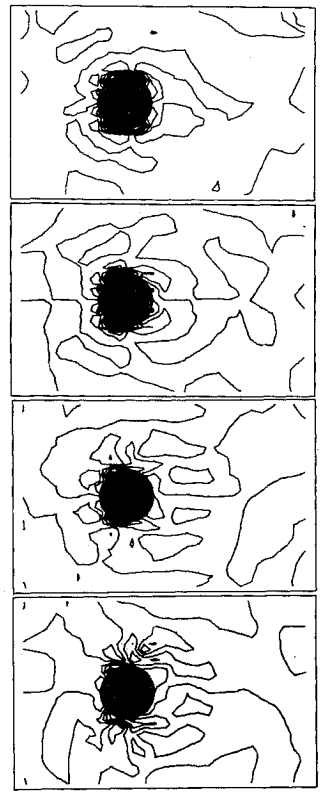

Fig. 5 Vorticity distribution around a circular cylinder ($Re = 10^4$, $t = 0.04, 0.30, 0.80, 1.10$).

The accuracy and stability of the numerical integration of the vorticity transport equation was analyzed as a function of the time step and the nonlinearity in the convection terms of Eq. (35). The instantaneous derivatives of the streamfunctions in Eq. (23), with respect to nodal vorticities, were obtained from the inverse of the matrix $\mathbf{S}^*$ in Eq. (29) and requires no additional computational effort.

Discussions

Sample Results

Sample results illustrating streamlines and vorticity and pressure distributions around a circular cylinder and a NACA 0012 airfoil are shown in Figs. 4–9. Starting from a zero vorticity distribution, the vorticity transport equation was integrated until

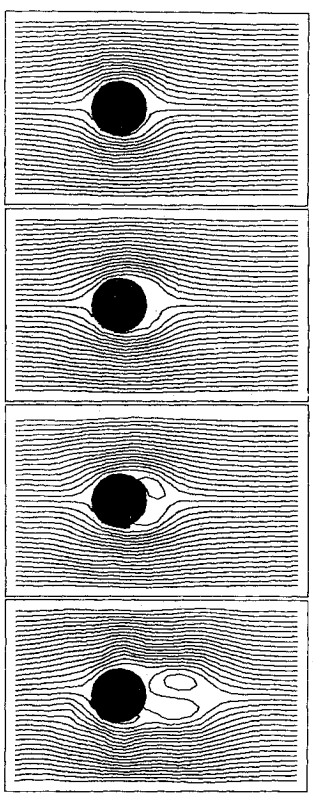

Fig. 4b Streamlines around a circular cylinder ($Re = 10^4$, $t = 0.14, 0.24, 0.30, 0.80$).

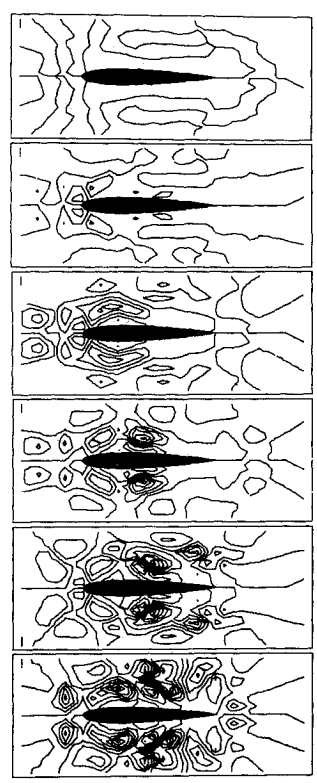

Fig. 6 Vorticity distribution around an airfoil ($Re = 10^3$, $\alpha = 0°, 0.07, 0.17, 0.215, 0.235$).

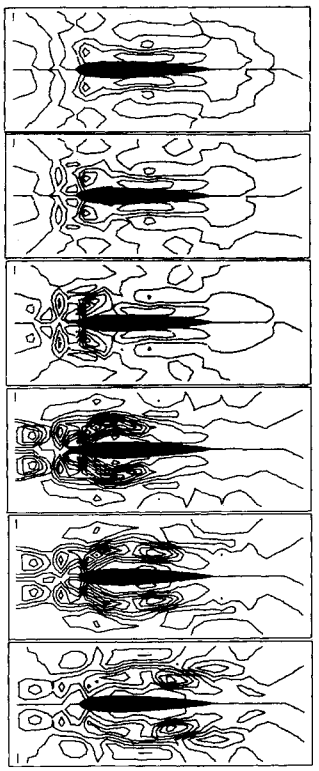

Fig. 7 Vorticity distribution around an airfoil ($Re = 10^5$, $\alpha = 0°$, $t =$ 0.03, 0.07, 0.13, 0.17, 0.215, 0.235).

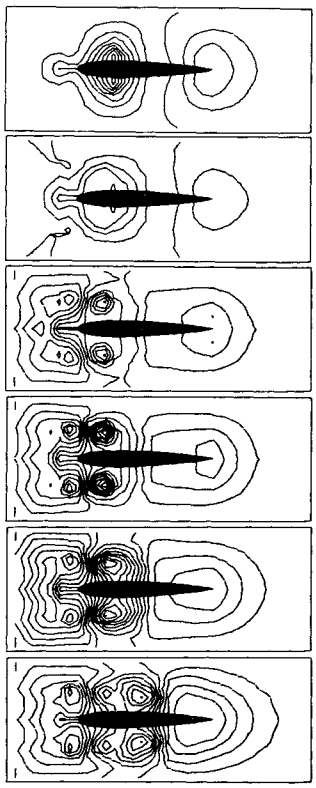

Fig. 9 Pressure distribution around an airfoil ($Re = 10^3$, $\alpha = 0°$, $t = 1.5$, 4.5, 8.0, 9.5, 11.5, 14.5).

a steady state was reached. Examples showing the oscillating instabilities of the flow in different flow regions are illustrated in Fig. 10. The sequence of streamline plots in Fig. 4 illustrates the development of the wake behind a cylinder at different Reynolds numbers. The generation of vorticities from the boundary of the obstacle can be observed from Figs. 5–7, showing vorticity diffusion characteristics at different Reynolds numbers.

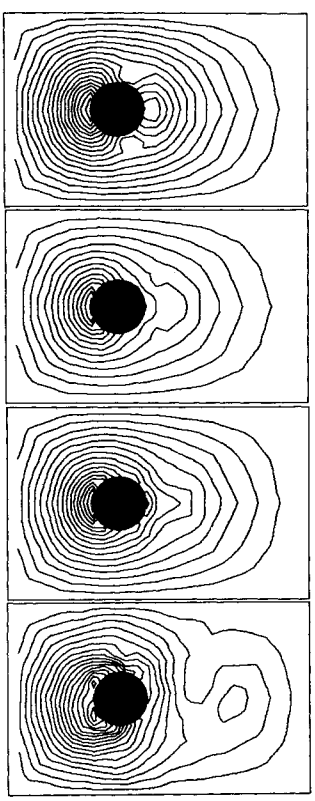

Fig. 8 Pressure distribution around a circular cylinder ($Re = 10^4$, $t = 0.1$, 0.3, 0.4, 1.1).

The contours in Figs. 8 and 9 show the effects of unsteady viscous flow characteristics on the pressure distribution around the obstacle. The variation of the surface pressure and vorticity distributions on the obstacle is shown in Fig. 11. From the pressure distribution near the trailing edge of the obstacle, one can observe a decrease in pressure due to the unsteady flow in the wake region. Figure 12 shows the vorticity distribution around an oscillating airfoil; starting from a steady-state condition around a NACA 0012 airfoil at $\alpha = 0°$, the vorticity transport equation was integrated as the airfoil was pitching.

Influence of Initial and Boundary Conditions

Instabilities occur at the initial steps of the numerical integration due to disturbances from the boundary conditions around the obstacle. To eliminate this problem an under-relaxation factor was applied for the first few steps of the numerical integration of Eq. (20).

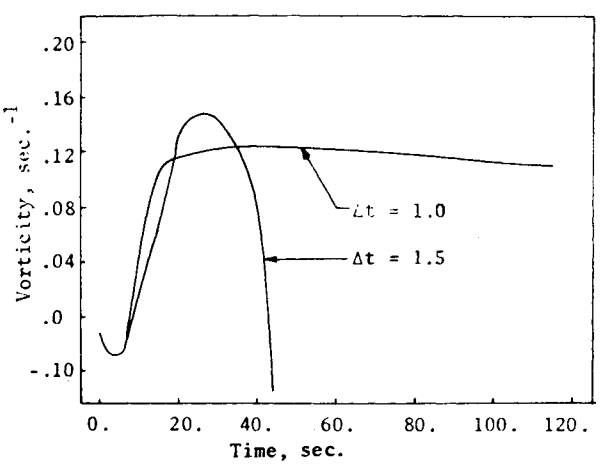

Fig. 10a Stability of the numerical integration of the vorticity transport equation for a Point B away from the obstacle ($Re = 40$).

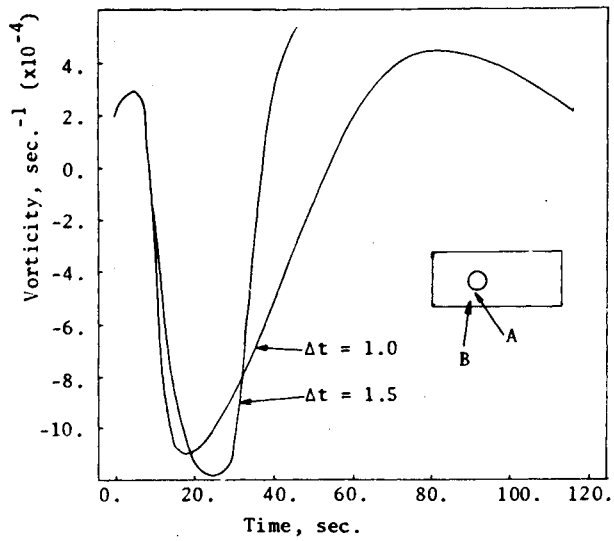

Fig. 10b Stability of the numerical integration of the vorticity transport equation for a point A near the obstacle ($Re = 40$).

Since pressures and vorticities were assumed to vary linearly inside a finite element, more than one constraint condition in a triangle causes linear dependence between these constraints. In the case of streamfunctions and velocities, up to three constraint conditions can be imposed for one triangular element. An insufficient number of points on the obstacle, at which boundary conditions are specified, may cause unsatisfactory results. For the case of moving obstacles, these instabilities must be considered when specifying boundary conditions for different positions of the obstacle.

Effiiciency of the Method of Solution

The computational cost depends on the number of nodal points in the finite element gridwork and on the number of constraint equations, specifying the boundary conditions. The partitioning of the matrices in Eqs. (28, 31, and 34) was arranged for an efficient solution. Considering three unknowns at each node of the finite element gridwork shown in Figs. 1 and 2, an

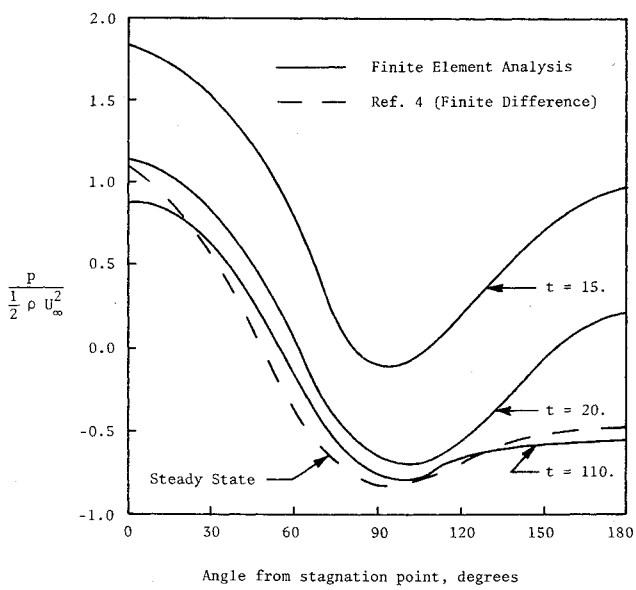

Fig. 11 Development of the surface pressure distribution on a circular cylinder ($Re = 40$).

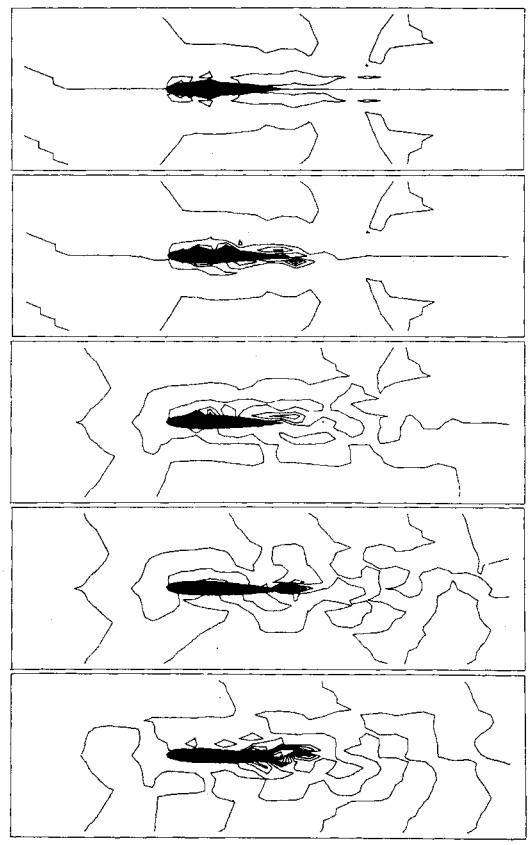

Fig. 12 Vorticity distribution about an oscillating NACA airfoil ($Re = 10^3$), $\hat{t} = 0.01$–0.05), ($\alpha = 0°$–$2.5°$).

inversion of the matrix $\mathbf{S}_s$, of order (458 × 458), was required for the solution of streamfunctions in Eq. (28). Matrix $\mathbf{S}_s$ and matrices $\mathbf{S}_p$ and $\mathbf{S}_\omega$, for the pressure and vorticity distributions, were inverted and stored at the beginning of the computational process. The matrices **b** and **e** for streamfunctions, vorticities, and pressures, representing the effect of the boundary conditions on the obstacle, were assembled at each time step in the computational procedure. For a UNIVAC 1108 computer with 65K core storage, the required computational time for various flow conditions are listed in Table 1.

Accuracy and Stability Considerations

The discretization errors involved in the numerical analysis can be classified as: errors from the solution of Poisson's equation (21) and errors from the numerical integration of the vorticity transport equation (20). The finite element solution of Poisson's equation has been developed by several investigators and applied to plane stress problems; the results were satisfactory. The accuracy of the solution depends basically on the number of nodal points in the finite element gridwork. The accuracy and stability of the numerical integration of the vorticity transport equation was investigated for different Reynolds numbers and different integration steps. As shown in Fig. 10 numerical

Table 1 Required computational time

Re	t	No. of time steps[a]	Computer time
40	1	110	7.5 min
1000	0.1	120	8.5 min
10000	0.01	300	15.5 min

[a] No. of steps to reach steady state.

instabilities occur at different flow regions depending on the size of the time step.

The stability of the numerical integration of the vorticity transport equation can be investigated from the stability of the system of linear equations

$$d\omega/dt = \mathbf{A}\omega \tag{38}$$

It can be shown that the necessary condition for the stability of the numerical integration of Eq. (38) can be expressed as

$$\Delta t \leqq 2/\delta_{\max} \tag{39}$$

where Δt is the integration time step and $\delta_{\max}$ is the maximum value of matrix **A**. An upper bound of $\delta_{\max}$ can be obtained from the largest eigenvalue of a single finite element triangle in the gridwork. For a typical triangular element, the eigenvalues γ_i can be calculated from the following equation

$$\left\{\begin{bmatrix}(vy_{23}/4A)+\frac{1}{24}(2u_1+u_2+u_3)\\(vy_{31}/4A)+\frac{1}{24}(u_1+2u_2+u_3)\\(vy_{12}/4A)+\frac{1}{24}(u_1+u_2+2u_3)\end{bmatrix}[y_{23}\,y_{31}\,y_{12}]\right.$$
$$\begin{bmatrix}(vx_{32}/4A)+\frac{1}{24}(2v_1+v_2+v_3)\\(vx_{13}/4A)+\frac{1}{24}(v_1+2v_2+v_3)\\(vx_{21}/4A)+\frac{1}{24}(v_1+v_2+2v_3)\end{bmatrix}[x_{32}\,x_{13}\,x_{21}]-$$
$$\left.\frac{\gamma_i A}{12}\begin{bmatrix}2&1&1\\1&2&1\\1&1&2\end{bmatrix}\right\}\begin{bmatrix}\omega_1\\\omega_2\\\omega_3\end{bmatrix}=\mathbf{0} \tag{40}$$

For a freestream flow u is constant and $v = 0$. For a triangular element with a base parallel to the direction of the freestream flow and with a height h, the largest eigenvalue becomes

$$\gamma_{\max} = 25.8v/h^2 \tag{41}$$

As can be seen from Eq. (41), the numerical integration of Eq. (38) becomes more stable for fluids with lower viscosity.

For a triangular element which has a base on the obstacle boundary ($u_1 = u_3 = v_1 = v_3 = 0$) and neglecting the vertical velocity v_2, the largest eigenvalue in Eq. (40) can be written as

$$\gamma_{\max} = 15(v/h^2)+[117(v/h^2)^2-6(v/h^2)(u_2/h)]^{1/2} \tag{42}$$

The stability of Eq. (38) depends on the real part of $\gamma_{\max}$ in Eq. (42). If the velocity term u_2 satisfies the expression

$$u_2 < 19.5\,v/h \tag{43}$$

$\gamma_{\max}$ is a real number. An upper bound of the time step of the numerical integration can be estimated from Eq. (39). However, if Eq. (42) is not satisfied, the solution of the numerical integration has an oscillatory behavior. Eq. (43) also shows that at the boundary-layer region, where the velocity distribution varies parabolically starting from the boundary of the obstacle, stable results can be obtained by using smaller triangles, and thus decreasing u_2 faster than h.

Conclusions

A general numerical method for the analysis of unsteady, incompressible and viscous flow around oscillating obstacles is presented. The method is flexible and can deal effectively with difficulties involved in practical unsteady flow analysis. The main points developed can be summarized as follows: a) a formulation of the time-dependent boundary conditions at an obstacle in a manner which provides computational efficiency, by allowing a stationary finite element grid; b) application of a perturbation technique for treatment of the nonlinearities in the variational formulation of the vorticity transport equation; c) application of higher-order finite elements for a consistent solution of the governing equations and in describing the boundary conditions. Thus, it appears that the developed numerical method is powerful when compared with existing finite-difference solution of aerodynamics problems, and is particularly suitable for oscillating airfoil problems.

References

[1] Cheng, S. I. and Rimon, Y., "Numerical Solution of a Uniform Flow Over a Sphere at Intermediate Reynolds Numbers," *The Physics of Fluids*, Vol. 12, No. 5, May 1969, p. 949.

[2] Harlow, F. H. and Amsden, A. A., "Fluid Dynamics: An Introductory Text," Rept. LA-4100, Feb. 1970, Los Alamos Scientific Lab., Los Alamos, N. Mex.

[3] Roache, P. J. and Mueller, T. J., "Numerical Solutions of Laminar Separated Flows," *AIAA Journal*, Vol. 8, No. 3, March 1970, p. 530.

[4] Thoman, D. C. and Szewczyk, A. A., "Time-Dependent Viscous Flow Over a Circular Cylinder," *The Physics of Fluids Supplement II*, Vol. 12, No. 12, Dec. 1969, p. 76.

[5] Zienkiewicz, O. C. and Cheung, Y. K., *The Finite Element Method in Structural and Continuum Mechanics*, 2nd ed., McGraw-Hill, New York, 1967.

[6] Tong, P., "The Finite Element Method for Fluid Flow," *Recent Advances in Matrix Methods of Structural Analysis and Design*, edited by R. H. Gallagher, Y. Yamada, and J. Tinsley Oden, The University of Alabama Press, University, Ala., 1971, p. 787.

[7] Skiba, E., Unny, T. E., and Weaver, D. S., "A Finite Element Solution For a Class of Two-Dimensional Viscous Fluid Dynamics Problems," *Computer Aided Engineering*, edited by G. M. L. Gladwell, University of Waterloo, Waterloo, Ontario, Canada, 1970, p. 493.

[8] Bratanow, T. and Ecer, A., "Finite Element Analysis and Computer Graphics Visualization of Flow Around Pitching and Plunging Airfoils," NASA Rept., to be published.

[9] Kobiske, M. H., "An Application of the Finite Element Method in Determining the Pressure Distribution Around Pitching and Plunging Rotor Blade Airfoils," Master's thesis, Aug. 1972, Univ. of Wisconsin-Milwaukee, Milwaukee, Wis.

[10] Bazeley, G. P., Cheung, Y. K., Irons, B. M., and Zienkiewicz, O. C., "Triangular Elements in Plate Bending-Conforming and Non-Conforming Solutions," *Proceedings of Conference on Matrix Methods and Structural Mechanics*, AFFDL-TR-66-80 Oct. 26–28, 1965, Wright-Patterson Air Force Base, Ohio, pp. 547–576.